nature photonics

LETTERS

PUBLISHED ONLINE: 10 APRIL 2017 | DOI: 10.1038/NPHOTON.2017.45

Integrated Cherenkov radiation emitter eliminating the electron velocity threshold

Fang Liu*†, Long Xiao†, Yu Ye, Mengxuan Wang, Kaiyu Cui, Xue Feng, Wei Zhang and Yidong Huang*

Cherenkov radiation[1–4] has played a key role in the discovery of some fundamental particles and physical phenomena, including anti-protons[5], J particles[6] and neutrino oscillations[4]. The electron energy (velocity) threshold required to generate Cherenkov radiation in a natural medium is greater than hundreds of keV (refs 3,4). Although various approaches have been adopted, high-energy electrons (tens of keV)[7] are still required to generate Cherenkov radiation experimentally. Here, we demonstrate, in hyperbolic metamaterial, that the electron velocity threshold for Cherenkov radiation can be eliminated. Based on this threshold-less Cherenkov radiation, the first integrated free-electron light source has been realized. Cherenkov radiation covering $\lambda_0 \approx 500$–900 nm is obtained with an electron energy of only ~0.25–1.4 keV, which is two to three orders of magnitude lower than in previous reports[3,7–9]. This work provides a way to achieve threshold-less Cherenkov radiation, opens up the possibility of exploring high-performance integrated free-electron light sources and optoelectronic devices, and offers a platform to study the interaction of flying electrons with nanostructures on chip.

Cherenkov radiation (CR) is the electromagnetic radiation emitted by a moving charge passing through a dielectric medium with a velocity above a certain threshold[1–4]. In the early twentieth century, the discovery and explanation of CR overturned the belief that no material body can move at a velocity exceeding the speed of light in a medium and that a uniformly moving charged particle does not radiate electromagnetic waves[4]. Cherenkov and two other scientists were awarded the Nobel Prize in Physics in 1958 for their outstanding work in this area[3,4]. Subsequently, several great discoveries[4–6] have been made with the help of CR. Even today, the interest in CR generation continues, especially in the study of how moving charged particles interact with different materials and structures[7,9–22].

To generate CR, the charge velocity u_0 must be higher than the phase velocity of light in the medium[2–4]. Cherenkov generated the radiation in water with a proton energy of hundreds of MeV (refs 3,4). Smith and Purcell found a way to reduce the electron energy to ~300 keV for CR in air by having electrons fly on gratings[8]. Lowering the electron energy further, or even eliminating the threshold to generate CR, has continued to attract much attention. Threshold-less CR has been predicted and studied theoretically in photonic crystals[11], anisotropic media[18], nanowire metamaterials[19,20] and other materials and structures[21,22]. However, the lowest electron energy to generate CR, reported experimentally up to now, is still higher than 20 keV (ref. 7) in the visible/infrared light regions.

Here, we report the first integrated threshold-less CR source with a planar electron emitter on hyperbolic metamaterial (HMM). It is demonstrated that, with low-energy electrons (0.25–1.4 keV), CR is generated in the range $\lambda_0 \approx 500$–900 nm. The electron energy generating CR experimentally is three orders of magnitude lower than that in natural media[3] and two orders lower than with artificial structures[7–9], and the output power of 200 nW is two orders of magnitude higher than that generated by high-energy electrons (tens to hundreds of keV) in nanostructures[7,23].

The proposed integrated CR emitter is sketched in Fig. 1a. The planar Mo electrodes emit an electron bunch that flies on top of the multilayer HMM with a gap d along the z direction. The electron bunch has a constant velocity u_0 (constant energy E). Figure 1b presents scanning electron microscopy (SEM) images of the Mo electrode tip, multilayer HMM and Au nanoslits. The electrons emitted by the planar Mo electrode fly a distance of 200 μm in the z direction, above and parallel to the surface of the HMM, with a gap d of only ~40 nm. Having the d value as small as possible is key for generating CR in HMM (for more details see Methods).

As we know, to generate CR in a conventional isotropic medium, the velocity of the charge u_0 should be larger than the phase velocity of the electromagnetic wave in that medium[2–4]:

$$u_0 > \frac{c}{n} = \frac{c}{\sqrt{\varepsilon}} \tag{1}$$

where c is the speed of light in vacuum, n is the refractive index of the medium and $\varepsilon = n^2$ is the permittivity. HMM has demonstrated interesting properties for imaging, sensing and light emission[24,25], which is ascribed to the opposite signs of the effective permittivity along different directions (that is, ε_x and ε_z along the x and z directions, respectively). To study CR in HMM, the evanescent field surrounding the electron bunch with wavevector $\beta = \omega/u_0$ (ref. 26) at frequency ω is considered as the incidence to the HMM slab. Unlike assuming that the electrons move inside a metamaterial[18–20], here the free electrons fly on top of the HMM surface. The following are found to apply (Supplementary Sections 2 and 3): (1) for Type I HMM ($\varepsilon_x < 0$, $\varepsilon_z > 0$), there is no electron bunch velocity u_0 threshold for the generation of CR; (2) for Type II HMM ($\varepsilon_x > 0$, $\varepsilon_z < 0$), the condition to generate CR can be derived as

$$\begin{cases} u_0 < \dfrac{c}{\sqrt{\varepsilon_x}} \\ \varepsilon_z < 0 \end{cases} \tag{2}$$

On comparing equation (2) with equation (1), it is astonishing to note that the sign of the inequality is reversed. The fabricated Au/SiO_2 multilayers shown in Fig. 1b can be treated as Type II HMM and, according to equation (2), CR could be generated, even though the electron energy is rather low.

The radiation of the CR emitter shown in Fig. 1 was measured at room temperature. The voltage between the cathode and anode (V_{ca}) could vary from ~0 to 10 kV, the pulse width was 10 μs, and the repetition rate was 1,000 Hz. Figure 2a shows that the white noise of the photodetector is ~2 nW, and the output power of

Department of Electronic Engineering, Tsinghua National Laboratory for Information Science and Technology, Tsinghua University, Beijing 100084, China. †These authors contributed equally to this work. *e-mail: liu_fang@tsinghua.edu.cn; yidonghuang@tsinghua.edu.cn

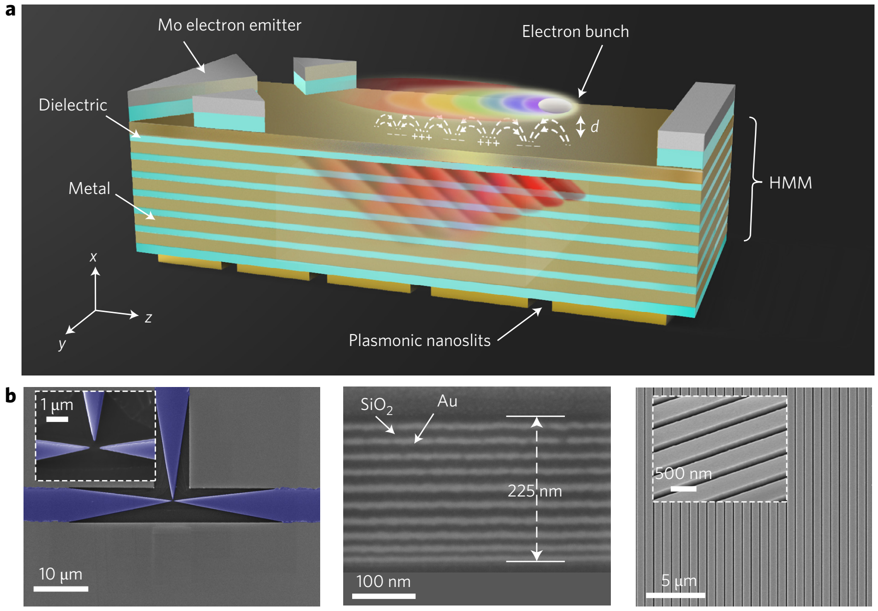

Figure 1 | The integrated CR emitter. **a**, Schematic of the CR emitter consisting of a planar Mo electron emitter, multilayer HMM and plasmonic periodic nanoslits. The HMM was formed by alternating Au (thickness h_m) and SiO_2 (thickness h_d) films. The Mo electrodes, including cathode, grid and anode, can emit free electrons from the cathode tip to anode by applying voltage. The plasmonic nanoslits couple the CR in the HMM to free space. **b**, SEM images of the CR emitter. Left: planar Mo electron emitter with tip radius smaller than 100 nm and thickness of 90 nm. Middle: HMM with h_m and h_d of ~10 nm. Right: periodic Au nanoslits with slit width of ~70 nm and period of ~570 nm. A 40-nm-thick SiO_2 layer between the Mo and multilayers controls the gap between the flying electrons and the chip surface. The distance between the cathode and anode is 200 µm, so free electrons can interact well with the HMM.

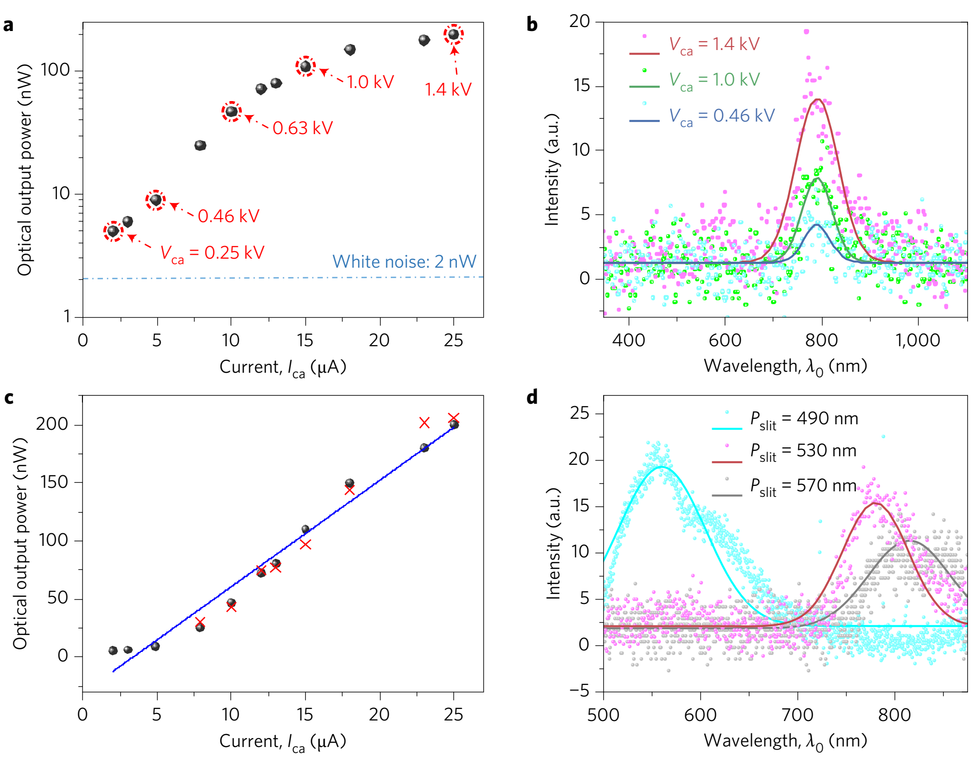

Figure 2 | Measured optical output of the integrated CR emitter. **a**, Optical output power of the chip with cathode–anode voltage V_{ca} (current I_{ca}) varying from 0.25 to 1.4 kV (cathode is 0 V, grid is 110 V) with a fixed plasmonic nanoslit period of P_{slit} = 530 nm. **b**, Spectra of output light when V_{ca} = 0.46, 1.0 and 1.4 kV. Symbols represent data from the spectrometer and curves are Gaussian fits. **c**, Optical output power versus cathode–anode current I_{ca}. Red crosses indicating the integral values of the Gaussian fitting curves of the measured spectra are in good agreement with the black symbols from **a**. **d**, Spectra of output light with different P_{slit}. Grey, red and turquoise curves/symbols correspond to P_{slit} = 570 nm (V_{ca} = 1.15 kV), 530 nm (V_{ca} = 1.4 kV) and 490 nm (V_{ca} = 1.35 kV), respectively.

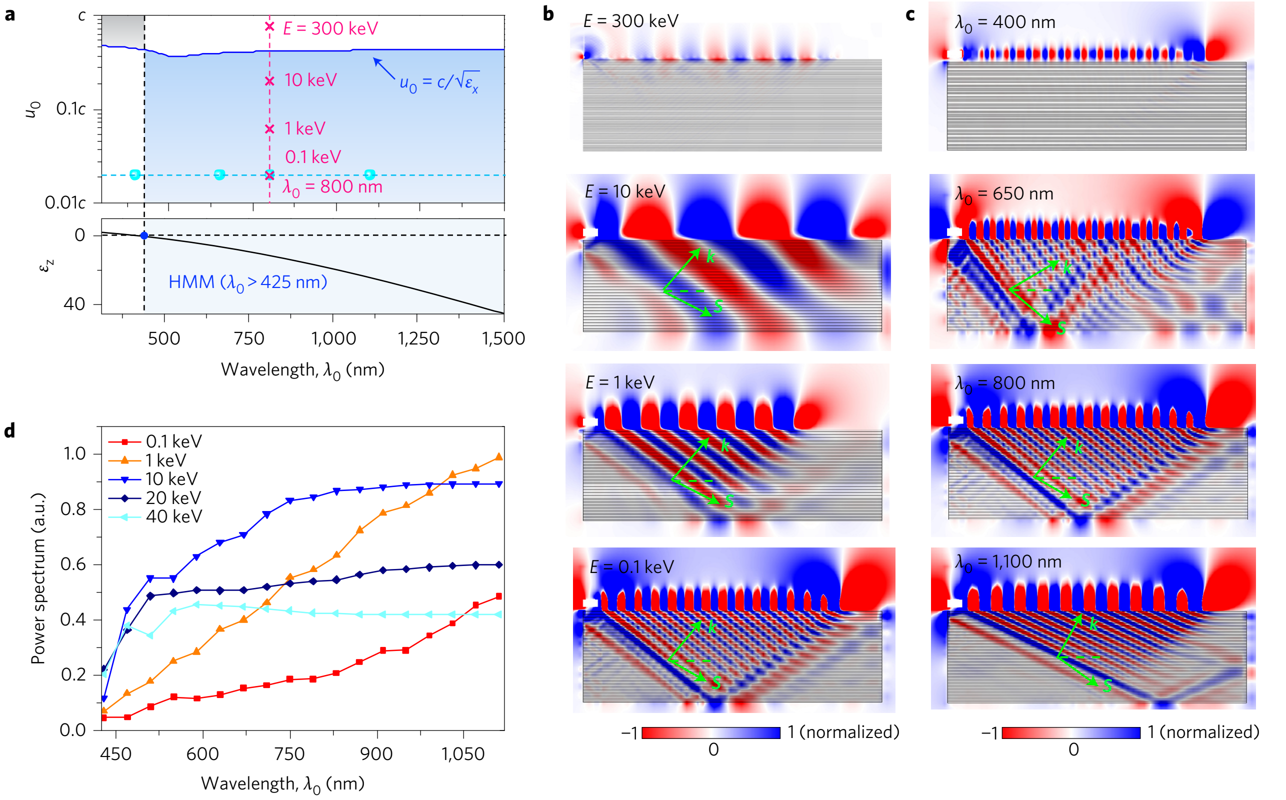

Figure 3 | Calculation of CR in HMM. a, The region of wavelength λ_0 and electron velocity u_0 for CR generation in multilayers. CR can be generated in the blue shaded area ($\lambda_0 > 425$ nm and $u_0 < c/\sqrt{\varepsilon_x}$) and the grey shaded area ($\lambda_0 < 425$ nm and $u_0 > c/\sqrt{\varepsilon_x}$). c is the light speed in vacuum. **b**, Numerical simulation of CR (electric field E_z) with $E = 0.1$, 1, 10 and 300 keV when $\lambda_0 = 800$ nm (corresponding to red crosses in **a**). **c**, Numerical simulation of CR (E_z) at $\lambda_0 = 400$, 650, 800, 1,100 nm when $E = 0.1$ keV (corresponding to turquoise dots in **a**). **d**, Simulated power spectrum of CR in HMM for different E. Here, $h_m = h_d = 2$ nm, $d = 40$ nm, the permittivities of Mo, Au and SiO_2 are taken from ref. 28, and the plasmonic periodic nanoslits are removed. The simulation is controlled for a short time (the reflection of CR on the bottom of the HMM is not obvious) to observe the phase front and radiation angle.

light originating from the CR emitter when $V_{ca} \approx 0.25$–1.4 kV ($I_{ca} \approx$ 2–25 μA) is obviously higher than the white noise. Although the electromagnetic wave in HMM could also be excited by a long-range Coulomb interaction[26], an additional experiment (Supplementary Section 10) showed that this effect is much weaker than CR and can be ignored here. In other words, we have confirmed that CR has been generated, even when V_{ca} is as low as 0.25 kV ($I_{ca} = 2$ μA). Taking $V_{ca} = 0.46$, 1.0 and 1.4 kV ($I_{ca} = 4.9$, 15 and 25 μA), for example, Fig. 2b presents light spectra covering the range $\lambda_0 \approx 700$–900 nm with a central wavelength around 780 nm. Because the radiation power of CR does not change significantly with E (namely V_{ca}) when E varies between 0.25 and 1.4 keV (Supplementary Fig. 5), the optical output power is mainly decided by and increases linearly with, I_{ca} (the number of electrons per unit time from cathode to anode). This is confirmed by Fig. 2c, which shows the linear increase of optical output power with I_{ca}. If I_{ca} could be maintained for a lower V_{ca} (lower u_0) by increasing the charge quantity, CR should be observed for even lower V_{ca}. The lowest electron energy allowing CR is decided by the thickness of the Au and SiO_2 layers (Supplementary Section 8).

Because the Au/SiO_2 multilayers can be treated as HMM over a wide frequency range, super-broadband CR should be obtained in the multilayers. With nanoslits with fixed parameters, CR in HMM (frequency range of more than 600 nm in theory) could be coupled to free space in a relatively narrower frequency range (~100 nm) and the central wavelength will mainly be decided by the period of the nanoslits, P_{slit} (Supplementary Section 7 and Supplementary Fig. 7). If we vary P_{slit}, CR in the HMM should be observed in a different wavelength range. This is indeed observed in Fig. 2d, where the light spectra have a similar profile but different central wavelength for different values of P_{slit}. We can thus conclude that CR corresponding to $\lambda_0 \approx 500$–900 nm has been generated in the Au/SiO_2 HMM. This is, in fact, the first free-electron light source with a broadband light output to be realized.

To help understand the above experimental results, the following calculations were carried out. Using the effective medium theory[27], ε_x and ε_z were derived and the multilayers were treated as Type II HMM when $\lambda_0 > 425$ nm (Supplementary Fig. 1). According to equation (2), the region of CR generation in the multilayers, as a function of wavelength λ_0 (frequency) and electron velocity u_0 (energy E), can be divided into different areas (Fig. 3a). In the blue-shaded area (where $\lambda_0 > 425$ nm and $u_0 < c/\sqrt{\varepsilon_x}$), CR can be generated, even when the electron energy is ultra-low. In the area where $\lambda_0 < 425$ nm, the multilayers become conventional anisotropic dielectrics, which still requires $u_0 > c/\sqrt{\varepsilon_x}$ for CR (grey-shaded region in Fig. 3a).

Numerical simulation based on particle-in-cell finite-difference time-domain approach is shown in Fig. 3b,c. With the wavelength fixed at $\lambda_0 = 800$ nm, for example, CR can be derived in HMM when the electron energy E (velocity u_0) is 0.1 keV, 1 keV and 10 keV. When $E = 300$ keV, no CR can be found in the multilayers because u_0 is larger than $c/\sqrt{\varepsilon_x}$. With fixed electron energy $E = 0.1$ keV, CR can be obtained in HMM at $\lambda_0 = 650$ nm, 800 nm and 1,100 nm. The top panel of Fig. 3c confirms that no radiation is generated with such a low electron energy, because the multilayers are no longer a HMM at $\lambda_0 = 400$ nm. Therefore, the validity of equation (2) and the measured wide-spectrum CR using the super-low electron energy shown in Fig. 2 are confirmed by the simulation results. Figure 3d illustrates the simulated radiation power spectrum for different E. When E is high, the evanescent field surrounding the electron bunch has strong coupling with the mode in the HMM, and the power spectrum is mainly decided by the local density of states of the HMM (Supplementary Section 5). When E is lower than 1 keV, the influence of gap d on the radiation efficiency might become significant, and the longer wavelength has higher radiation efficiency.

The above results demonstrate the generation of CR in HMM when V_{ca} is only 0.25–1.4 kV. This indicates the following: (1) light emission is obtained with two to three orders of magnitude lower electron energy compared with previous reports[3,7–9] and (2) elimination of the velocity threshold for CR is possible. Moreover, benefitting from the threshold-less CR, the first integrated free-electron light source has been realized by integrating a planar electron emitter on HMM. Although less than 1% of the light energy could be coupled to free space (Supplementary Section 7), the measured output light power still reaches 200 nW, which is two orders of magnitude higher than any free-electron light source constructed using other nanostructures[7,23]. Elimination of the charge velocity threshold and the high radiation efficiency provide the possibility of not only enhancing existing devices (that is, extending the measurement range of Cherenkov counters[4]), but also making use of the super-wideband evanescent field surrounding flying electrons on chip (for realizing ultraviolet and broadband terahertz light sources) by designing appropriate HMM structures. Moreover, such an integrated CR emitter brings CR from the field of high-energy physics to integrated devices. It also provides a platform for studying the interaction between the flying electrons and other artificial nanostructures on chip, and more integrated vacuum optoelectronic devices could be expected in the future.

Methods

Methods and any associated references are available in the online version of the paper.

Received 18 July 2016; accepted 3 March 2017;
published online 10 April 2017

References

1. Cherenkov, P. Visible emission of clean liquids by action of gamma radiation. *Dokl. Akad. Nauk* **2,** 451 (1934).
2. Landau, L. D. & Lifshitz, E. M. *Electrodynamics of Continuous Media* 2nd edn (Pergamon, 1984).
3. Cherenkov, P. in *Nobel Lectures, Physics: 1942–62* (ed. Nobel Foundation Staff) 426–440 (Elsevier, 1964).
4. Bolotovskii, B. M. Vavilov–Cherenkov radiation: its discovery and application. *Phys. Uspekhi* **52,** 1099–1110 (2009).
5. Chamberlain, O., Segrè, E., Wiegand, C. & Ypsilantis, T. Observation of antiprotons. *Phys. Rev.* **100,** 947–950 (1955).
6. Aubert, J. J. *et al.* Experimental observation of a heavy particle J. *Phys. Rev. Lett.* **33,** 1404–1406 (1974).
7. Adamo, G. *et al.* Light well: a tunable free-electron light source on a chip. *Phys. Rev. Lett.* **103,** 113901 (2009).
8. Smith, S. & Purcell, E. Visible light from localized surface charges moving across a grating. *Phys. Rev.* **92,** 1069 (1953).
9. So, J.-K., García de Abajo, F. J., MacDonald, K. F. & Zheludev, N. I. Amplification of the evanescent field of free electrons. *ACS Photon.* **2,** 1236–1240 (2015).
10. Stevens, T. E., Wahlstrand, J. K., Kuhl, J. & Merlin, R. Cherenkov radiation at speeds below the light threshold: phonon-assisted phase matching. *Science* **291,** 627–630 (2001).
11. Luo, C., Ibanescu, M., Johnson, S. G. & Joannopoulos, J. D. Cerenkov radiation in photonic crystals. *Science* **299,** 368–371 (2003).
12. Cook, A. M. *et al.* Observation of narrow-band terahertz coherent Cherenkov radiation from a cylindrical dielectric-lined waveguide. *Phys. Rev. Lett.* **103,** 095003 (2009).
13. Xi, S. *et al.* Experimental verification of reversed Cherenkov radiation in left-handed metamaterial. *Phys. Rev. Lett.* **103,** 194801 (2009).
14. Chen, H. & Chen, M. Flipping photons backward: reversed Cherenkov radiation. *Mater. Today* **14,** 34–41 (2011).
15. Ren, H., Deng, X., Zheng, Y., An, N. & Chen, X. Nonlinear Cherenkov radiation in an anomalous dispersive medium. *Phys. Rev. Lett.* **108,** 223901 (2012).
16. Liu, S. *et al.* Surface polariton Cherenkov light radiation source. *Phys. Rev. Lett.* **109,** 153902 (2012).
17. Ginis, V., Danckaert, J., Veretennicoff, I. & Tassin, P. Controlling Cherenkov radiation with transformation-optical metamaterials. *Phys. Rev. Lett.* **113,** 167402 (2014).
18. Galyamin, S. N. & Tyukhtin, A. V. Electromagnetic field of a charge traveling into an anisotropic medium. *Phys. Rev. E* **84,** 056608 (2011).
19. Vorobev, V. V. & Tyukhtin, A. V. Nondivergent Cherenkov radiation in a wire metamaterial. *Phys. Rev. Lett.* **108,** 184801 (2012).
20. Fernandes, D. E., Maslovski, S. I. & Silveirinha, M. G. Cherenkov emission in a nanowire material. *Phys. Rev. B* **85,** 155107 (2012).
21. So, J. *et al.* Cherenkov radiation in metallic metamaterials. *Appl. Phys. Lett.* **97,** 151107 (2010).
22. Galyamin, S. N., Kapshtan, D. Y. & Tyukhtin, A. V. Electromagnetic field of a charge moving in a cold magnetized plasma. *Phys. Rev. E* **87,** 013109 (2013).
23. Adamo, G. *et al.* Electron-beam-driven collective-mode metamaterial light source. *Phys. Rev. Lett.* **109,** 217401 (2012).
24. Poddubny, A., Iorsh, I., Belov, P. & Kivshar, Y. Hyperbolic metamaterials. *Nat. Photon.* **7,** 948–957 (2013).
25. Yang, X., Yao, J., Rho, J., Yin, X. & Zhang, X. Experimental realization of three-dimensional indefinite cavities at the nanoscale with anomalous scaling laws. *Nat. Photon.* **6,** 450–454 (2012).
26. García de Abajo, F. J. Optical excitations in electron microscopy. *Rev. Mod. Phys.* **82,** 209–275 (2010).
27. Sihvola, A. *Electromagnetic Mixing Formulas and Applications* (Institution of Engineering and Technology, 1999).
28. Palik, E. D. *Handbook of Optical Constants of Solids* (Academic, 1985).

Acknowledgements

The authors thank J. Feng, G. Bai and X. Li in Beijing Vacuum Electronics Research Institute for help in testing the chip. The authors also thank Y. Zhang and A. Lambert for polishing the English. This work was supported by the National Basic Research Programs of China (973 Program) under contract no. 2013CBA01704 and the National Natural Science Foundation of China (NSFC-61575104 and 61621064).

Author contributions

F.L. proposed the idea of CR in HMM and directed L.X., Y.Y. and M.W. for the research work. F.L. and L.X. performed the theoretical study. F.L., L.X., Y.Y. and M.W. performed the numerical simulations. F.L., L.X. and Y.H. designed the device and experiment. F.L., L.X., Y.Y. and M.W. fabricated the samples and carried out the measurements. F.L., L.X., Y.Y., M.W., K.C., X.F., W.Z. and Y.H. discussed the results. F.L., L.X. and Y.H. wrote the manuscript, which was revised by all authors. F.L. and Y.H. led the overall direction of the project.

Additional information

Supplementary information is available in the online version of the paper. Reprints and permissions information is available online at www.nature.com/reprints. Publisher's note: Springer Nature remains neutral with regard to jurisdictional claims in published maps and institutional affiliations. Correspondence and requests for materials should be addressed to F.L. and Y.H.

Competing financial interests

The authors declare no competing financial interests.

Methods

Key to generate CR in HMM experimentally. Although our theoretical and simulation results predict that CR in HMM is possible at ultralow electron energies, to realize CR in HMM experimentally is still very difficult. This is because the evanescent electromagnetic field is tightly bounded by the surrounding flying electrons when the electron energy is low (that is, when $E = 1$ keV, the electromagnetic field in the visible region decays to one-tenth at a distance of only tens of nanometres away from the electron trace). In experiments, the most challenging aspect is to manipulate the electrons to fly in a parallel manner above the surface of the HMM with a height of just tens of nanometres, which is extremely hard when introducing free electrons from outside the chip. Here, the problem was solved perfectly by integrating the planar electron emitter with the HMM structure. The planar electron emitter ensures that the trace of the flying electrons is parallel to the chip surface. In addition, the Au and SiO_2 layer should be thin and smooth enough that a CR mode with large effective refractive index (excited by electrons with low energy) can be supported in the multilayers (Supplementary Section 8).

Sample fabrication. Transparent quartz (KJ Group) with high smoothness (surface roughness below 0.5 nm) was selected as the substrate. A plasmonic grating with a period of 570 nm and slot width of 60 nm was realized on the substrate by sputtering a 100-nm-thick Au layer then etching with a focused ion beam (FIB). A PMMA polymer layer with a thickness of ~50–70 nm was applied to cover the Au grating to create a smooth chip surface for further multilayer preparation. Ten pairs of Au (~10-nm-thick) and SiO_2 (~10-nm-thick) layers were then sputtered alternately to form the multilayer HMM structure. Finally, the integrated planar electron emitter was fabricated on top. Followed by ultraviolet lithography, 40-nm-thick SiO_2 and 90-nm-thick Mo sputtering and a liftoff process, FIB milling was used to sharpen the tip of the cathode and grid electrode. The 40-nm-thick SiO_2 layer between the Mo and Au layers ensured the insulation of the Mo electrodes and controlled the gap between the flying electrons and the surface of the HMM.

To ensure the electrons could be extracted under low voltage, the parameters of the Mo electrode were controlled carefully. (1) The thickness of the Mo layer was controlled to be ~90 nm. A thinner Mo layer would result in higher resistance and the electrode would be destroyed easily by discharging, while a thicker Mo layer would lead to the requirement for a higher voltage for electron emission. (2) The radius of curvature of the electron tip should be less than 100 nm. This sharp tip ensures electron emission under low voltage. (3) The distance between the cathode and grid should be only ~300 nm. Such a small distance ensures a high electric field when the cathode–grid voltage is only 110 V, and electrons can be extracted easily from the cathode.

Measurement set-up. Supplementary Fig. 9 presents the measurement set-up. To avoid the influence of air on electron emission, the chip was placed in a high-vacuum chamber (2×10^{-6} Pa). Similar to CR generation with high-energy electrons[29,30], a voltage pulse was applied between the cathode and anode (V_{ca}); this varied from 0 to 10 kV with a pulse width of 10 μs and a repetition rate of 1,000 Hz. The current I_{ca} from cathode to anode increased with V_{ca}. A parabolic mirror plated with a silver layer on its inner surface was used to collect the light from the vacuum chamber through its quartz window. The chip was placed at the focal point of the parabolic mirror. Outside the chamber, a lens was applied to gather the light into the fibre for measurement by a spectrometer (Ocean Optics QE65PRO) and a power meter (Thorlabs S130VC). Unlike previous studies, which used a liquid-nitrogen-cooled charge-coupled device array detector for light spectra measurements[7,9,23], we simply used a semiconductor-cooled spectrometer and could obtain an obvious spectra output, indicating that the output power of our device is much stronger than that achieved in previous reports[7,9,23].

Measurement of optical output power. The optical output power measured by the power meter was recorded by a data acquisition card every 10 s, and more than ten values were obtained for each V_{ca}. The data shown in Fig. 2a are the average output power, and the standard deviation is less than 4% of the average value. Because the fluctuation (standard deviation) of the output power is rather small, error bars are not shown in Fig. 2a.

Measured spectrum fitting. Light spectra coupled to free space from the multilayers were simulated (Supplementary Section 7 and Supplementary Fig. 7). Meanwhile, for simplicity, we used a Gaussian curve to fit the measured light spectra in Fig. 2. Although the noise of the spectra in Fig. 2 is a little high, the integral value of the fitting curves in Fig. 2b (red crosses in Fig. 2c) is in good agreement with the measured total output power (black dots in Fig. 2c) when the current I_{ca} (voltage V_{ca}) is different, which means that the Gaussian curve is appropriate for measured spectrum fitting.

Data availability. Most of the data that support the plots can be found within this paper and the Supplementary Information. Other data are available from the corresponding author upon reasonable request.

References

29. Garate, E., Cook, R., Heim, P., Layman, R. & Walsh, J. Čerenkov maser operation at lower-mm wavelengths. *J. Appl. Phys.* **58,** 627–632 (1985).
30. Felch, K. L., Busby, K. O., Layman, R. W., Kapilow, D. & Walsh, J. E. Cerenkov radiation in dielectric-lined waveguides. *Appl. Phys. Lett.* **38,** 601–603 (1981).